Lecture 7

Faults and Fractures at Depth
(22 April 2020)

Ki-Bok Min, PhD

Professor
Department of Energy Resources Engineering
Seoul National University

SEOUL NATIONAL UNIVERSITY

Faults and Fractures at Depth
Introduction

SEOUL NATIONAL UNIVERSITY

- Importance
  - Hydraulic properties - Major conduits for fluid flow
  - Mechanical properties
  - Wellbore Stability
  - Limits in situ stress

- Basic tools
  - 3D Mohr Circle
  - Stereonet
  - Focal mechanism
- Nomenclature
  - Fault
    - Planar discontinuities associated with shear deformation
  - Fracture
    - Planar discontinuities in opening model (without shear deformation)

Representation of fracture and fault data at depth

SEOUL NATIONAL UNIVERSITY

- Dip/Dip direction or Dip/Strike
  - Dip angle: angle between the steepest line and horizontal plane
  - Dip direction: bearing of this steepest line measured from North (clockwise)
    - Ex) 130/50 (dip direction/dip)
  - Dip & Strike (주향)
    - Ex) strike N40E, dip 50SE
- Rake
  - Slip direction measured from the plane of the fault from horizontal

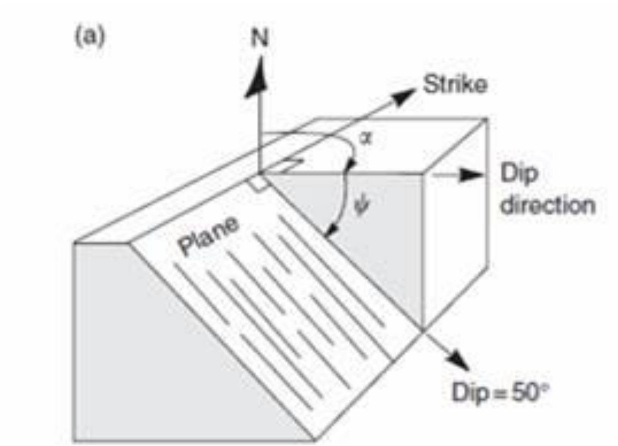

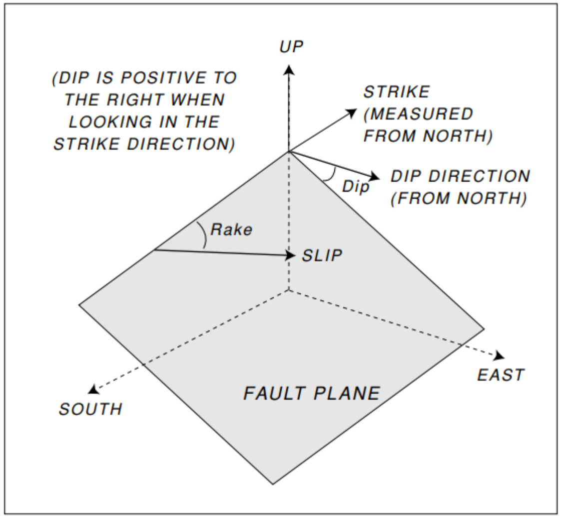

Figure 5.5. Definition of strike, dip and dip direction on an arbitrarily oriented planar feature such as a fracture or fault. Rake is the direction of slip in the plane of the fault as measured from horizontal.

Zoback MD, 2007, Reservoir Geomechanics, Cambridge University Press

Representation of fracture and fault data at depth
Stereographic lower hemisphere projection

SEOUL NATIONAL UNIVERSITY

- Stereographic lower hemisphere projection
  - show the trace of a fracture plane (where it intersects the lower half of the hemisphere) or
  - the intersection of fracture poles (normals to the fracture planes) and the hemisphere
- The circular diagrams (Figure 5.6b) used to represent such projections: stereonet

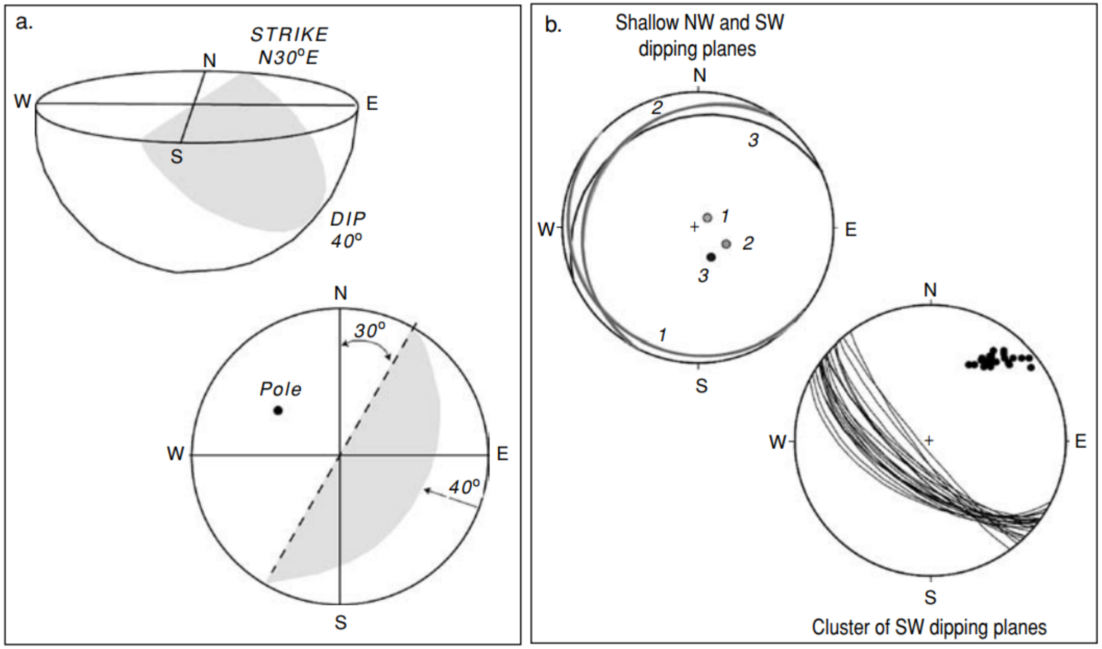

Figure 5.6. Illustration of the display of fracture and fault data using lower hemisphere stereographic projections. Either the intersection of the plane with the hemisphere can be shown or the pole to the plane. Planes which are sub-horizontal have poles that plot near the center of the stereonet whereas steeply dipping planes have poles which plot near the edge.

Zoback MD, 2007, Reservoir Geomechanics, Cambridge University Press

Representation of fracture and fault data at depth

SEOUL NATIONAL UNIVERSITY

- Tadpole plot: (tail = dip direction)
- Stereonet
- Contour plot on stereonet
- Rose diagram

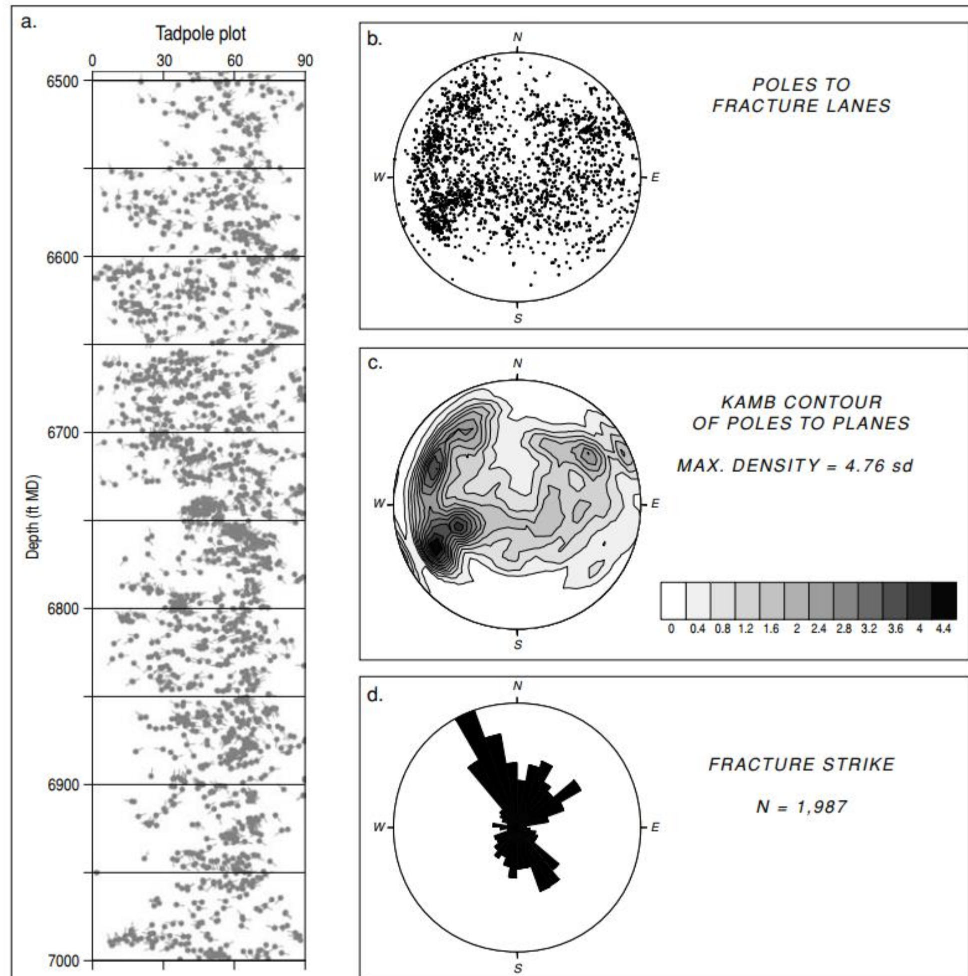

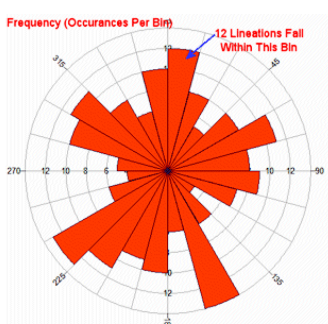

Zoback MD, 2007, Reservoir Geomechanics, Cambridge University Press

Representation of fracture and fault data at depth

SEOUL NATIONAL UNIVERSITY

- Fractures are prevalent, and with various orientations and sizes

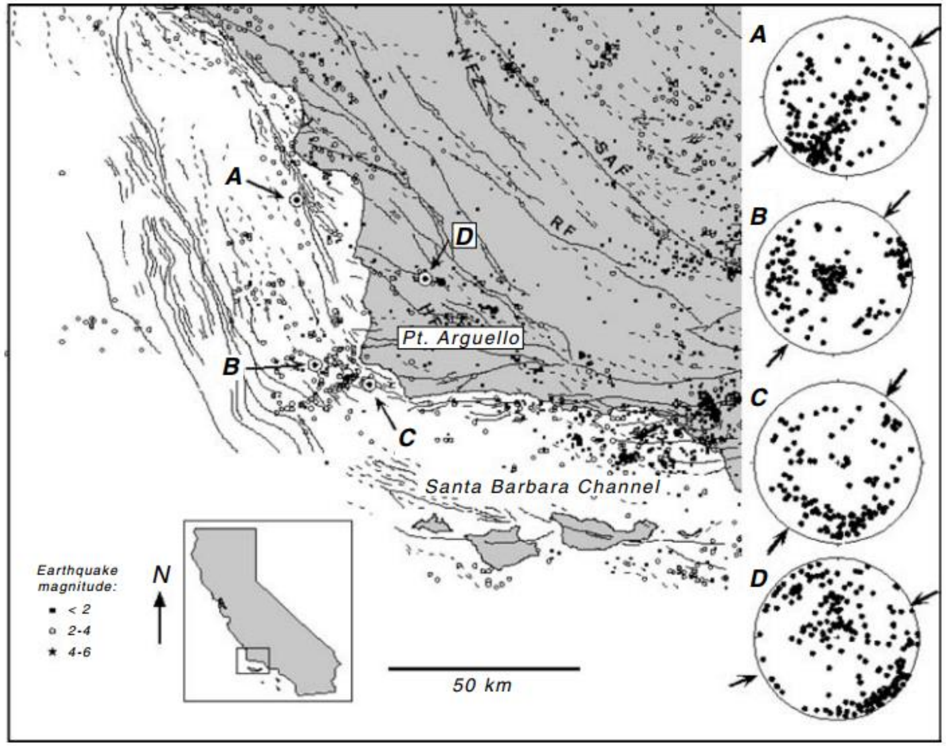

Figure 5.8. The Point Arguello area in western California is characterized by numerous earthquakes (dots), active faults and folds (thin lines). Image data from four wells drilled into the Monterey formation (A,B,C,D) illustrate the complex distribution of faults and fractures in each as shown in the stereonets (after Finkbeiner, Barton *et al.* 1997). *AAPG© 1997 reprinted by permission of the AAPG whose permission is required for futher use.*

Zoback MD, 2007, Reservoir Geomechanics, Cambridge University Press

Representation of fracture and fault data at depth
Characterization

- Geometrical properties of fractures
  - Orientation (dip and dip direction), size (trace length in 2D), density (spacing in parallel infinite fracture), location, aperture, roughness
- Characterization method
  - Exposed rock faces
    - scanline sampling: line-based sample, use measuring tape (줄자).
    - Window sampling: area-based sample, rectangle of measuring tapes
  - Borehole sampling
- Geometric model of fractured rock – deterministic or stochastic generation of fractures
  - Monte Carlo Simulation

Outcrop of granite (Forsmark, Sweden, 2004)

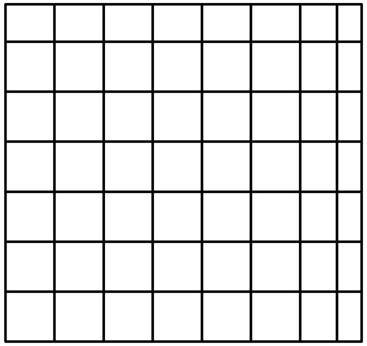

Idealized regular fracture model

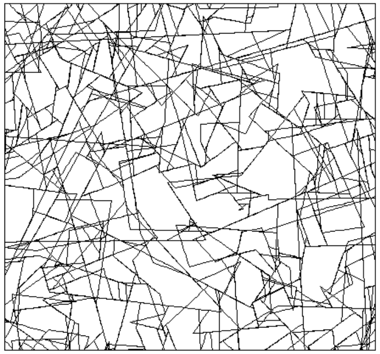

Discrete Fracture Network (암반균열망)

Faults and Fractures at Depth
Introduction

- Schematics of the fractures with respect to in situ stress orientation

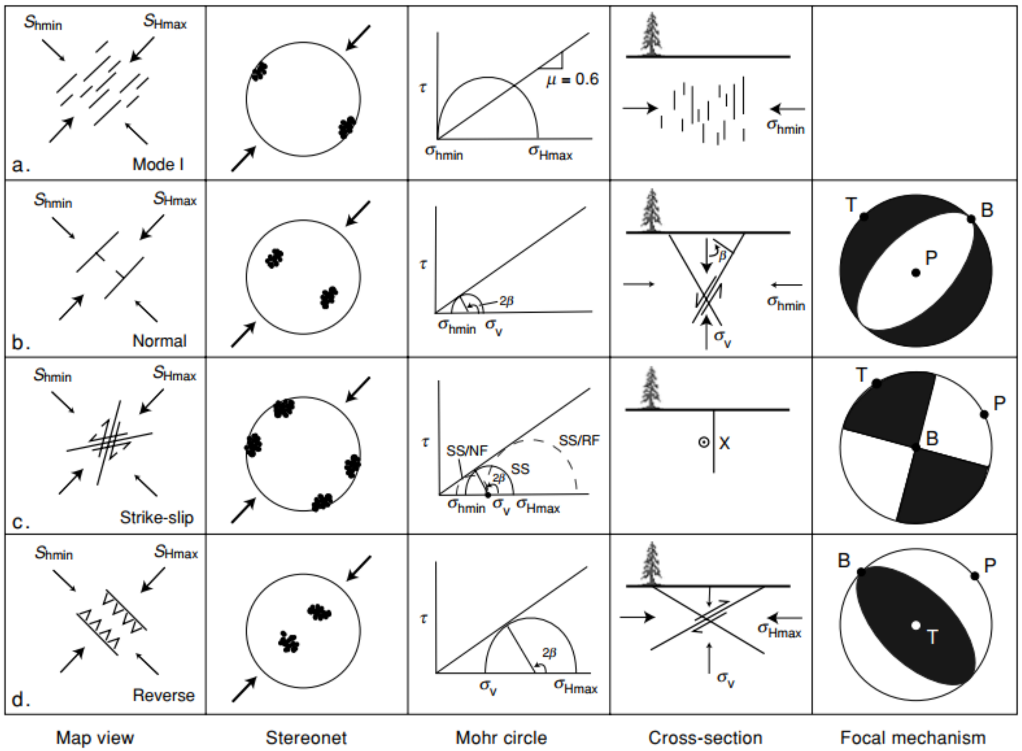

Figure 5.1. Schematic illustration of the orientation of various types of fractures and faults with respect to the orientation of S_{Hmax} and S_{hmin}. (a) Mode I fractures and joints are expected to form parallel to S_{Hmax} and normal to S_{hmin}. (b) Conjugate strike-slip faults are expected to be vertical and strike ~30° from the direction of S_{Hmax} (for $\mu \sim 0.6$). (c) Reverse faults are expected to dip ~30° (for $\mu \sim 0.6$) and strike normal to the direction of S_{Hmax}. (d) Conjugate normal faults are expected to dip ~60° (for $\mu \sim 0.6$) and strike parallel to the direction of S_{Hmax}. Because fractures and faults are introduced during multiple deformational episodes (depending on the age and geologic history of the formation) it is common for formations to contain numerous fractures at a variety of orientations.

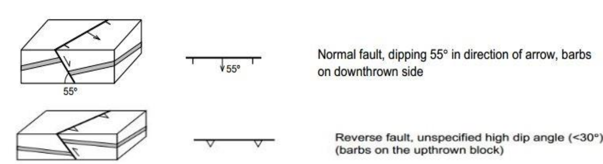

Zoback MD, 2007, Reservoir Geomechanics, Cambridge University Press

Fracture Mode I, II and III

- Crack-tip deformation mode
  - Mode I: crack opening model – mostly relevant to Hydraulic Fracturing
  - Mode II: sliding (shearing) model
  - Mode III: tearing model

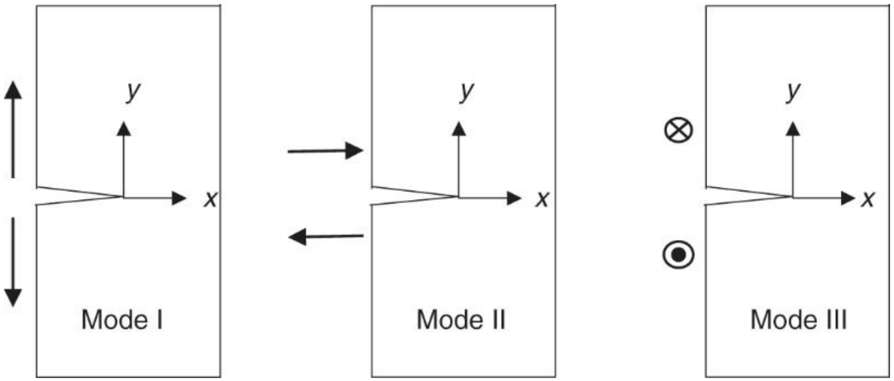

Jaeger, Cook & Zimmerman, 2007, Fundamentals of Rock Mechanics, 4th ed, Blackwell Publishing

Faults, Fractures and Fluid Flow
Cubic's law

SEOUL NATIONAL UNIVERSITY

Real rock fracture

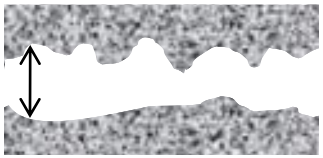

Idealization

Conceptual model

Idealized rock fracture

Aperture (e, or b): size of opening measured normal to the fracture wall

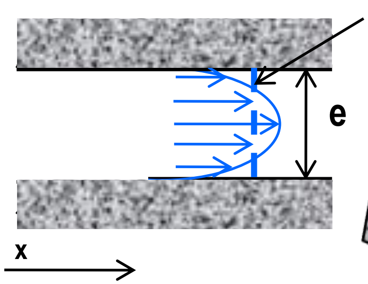

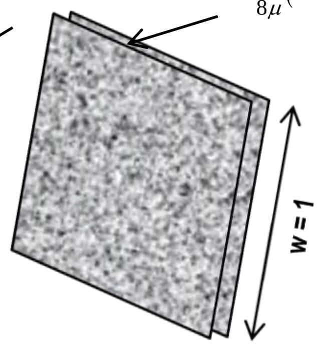

$$v = -\frac{1}{8\mu}\left(e^2 - 4y^2\right)\frac{d(\rho_w g h)}{dx}$$

$$Q = \int_{-\frac{e}{2}}^{\frac{e}{2}} v(w\,dy) = -\frac{we^3}{12\mu}\frac{d}{dx}(\rho_w g h)$$

$$Q = -\frac{e^3}{12\mu}\frac{d}{dx}(\rho_w g h) = -\frac{\rho_w g e^3}{12\mu}\frac{dh}{dx}$$

$$\boxed{Q = -\frac{\rho_w g e^3}{12\mu}\frac{\partial h}{\partial x}}$$

$$\boxed{Q = -\frac{e^3}{12\mu}\frac{\partial p}{\partial x}}$$

← **with zero elevation**

ρ_w: density of fluid
g: acceleration of gravity
μ: viscosity (=η)

– Cubic law: for a given gradient in pressure and unit width (w), flow rate through a fracture is proportional to the **cube** of the fracture aperture.

plate approximation for fluid flow through a planar fracture. For a given fluid viscosity, η, the volumetric flow rate, Q, resulting from a pressure gradient, ∇P, is dependent on the cube of the separation between the plates, b,

$$Q = \frac{b^3}{12\eta}\nabla P \tag{5.1}$$

Faults, Fractures and Fluid Flow
Mode I fracture

SEOUL NATIONAL UNIVERSITY

- Maximum separation (b_{max}) at the mid point with crack length L with elliptical cross-section

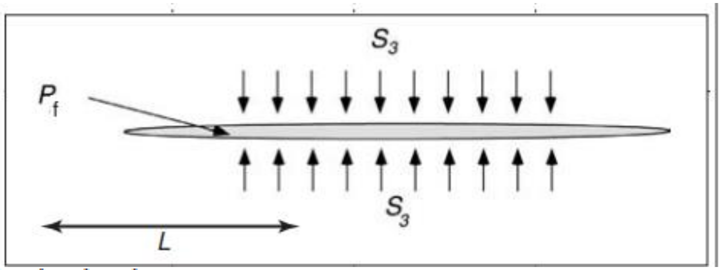

Figure 4.21). The maximum separation aperture of the fracture at its midpoint is given by

$$b_{\max} = \frac{2(P_f - S_3)L(1 - \nu^2)}{E} \qquad (5.2)$$

where P_f is the fluid pressure in the fracture, ν is Poisson's ratio and E is Young's modulus. This results in a flow rate given by

modulus. This results in a flow rate given by

$$Q = \frac{\pi}{8\eta}\left(\frac{b_{\max}}{2}\right)^3 \nabla P \qquad (5.3)$$

$$Q = \frac{b^3}{12\eta}\nabla P$$

which yields

$$Q = \frac{\pi}{8\eta}\left[\frac{L(1 - \nu^2)(P_f - S_3)}{E}\right]^3 \nabla P \qquad (5.4)$$

Zoback MD, 2007, Reservoir Geomechanics, Cambridge University Press

Faults, Fractures and Fluid Flow

Mode I fracture

- Parallel plate model
  - Flow rate through a fracture in response to a pressure gradient ~ cube of the aperture (b)

$$Q = \frac{b^3}{12\eta} \nabla P$$

- Fracture with elliptical cross section
  - Flow rate through a fracture in response to a pressure gradient ~ cube of the $L^*(P_p - S_3)$

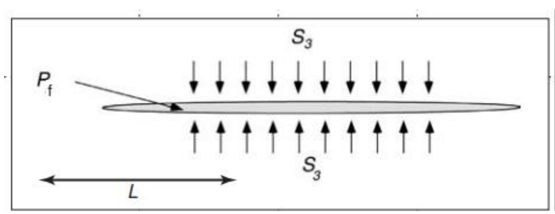

$$Q = \frac{\pi}{8\eta} \left(\frac{b_{\max}}{2} \right)^3 \nabla P$$

$$Q = \frac{\pi}{8\eta} \left[\frac{L(1 - \nu^2)(P_f - S_3)}{E} \right]^3 \nabla P$$

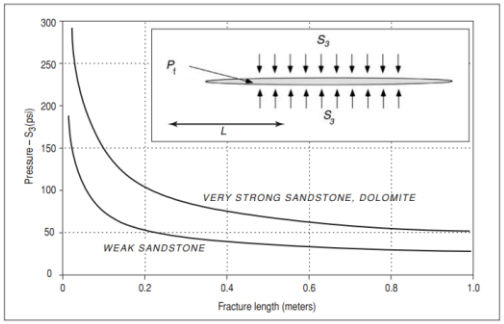

Figure 4.21. The difference between internal fracture pressure and the least principal stress as a function of fracture length for a Mode I fracture (see inset) for rocks with extremely high fracture toughness (such as very strong sandstone or dolomite) and very low fracture toughness (weakly cemented sandstone).

  - Significant aperture may not be possible in Mode I
    - Fracture propagation will drop the pressure
  - Effect of shearing/sliding will be much greater

Zoback MD, 2007, Reservoir Geomechanics, Cambridge University Press

Faults, Fractures and Fluid Flow
Faults (with shear)

SEOUL NATIONAL UNIVERSITY

- Faults are main conduit for fluid flow
  - Enhancement of permeability in fault is critically important for hydrocarbon production and fluid flow in general.

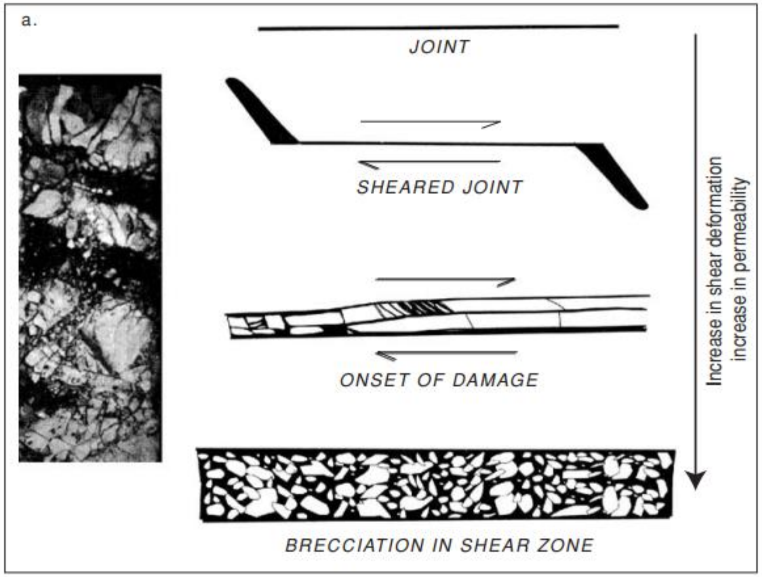

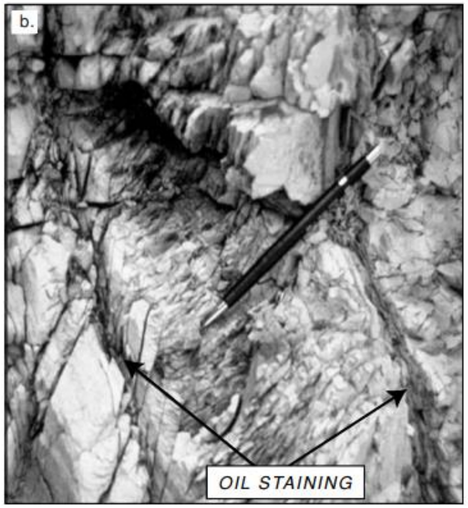

Figure 5.2. Schematic illustration of the evolution of a fault from a joint (after Dholakia, Aydin *et al*. 1998). As shear deformation occurs, brecciation results in interconnected porosity thus enhancing formation permeability. In the Monterey formation of California, oil migration is strongly influenced by the porosity generated by brecciation accompanying shear deformation on faults. This can be observed at various scales in core (a) and outcrop (b). *AAPG© 1998 reprinted by permission of the AAPG whose permission is required for futher use.*

Zoback MD, 2007, Reservoir Geomechanics, Cambridge University Press

Wellbore Imaging

SEOUL NATIONAL UNIVERSITY

- Wellbore imaging device:
  - Direct information on the distribution and orientation of fractures
  - Detailed cross-sectional shape of the wellbore wall

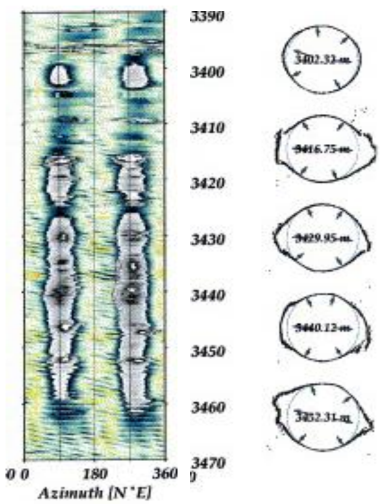

Detailed cross section

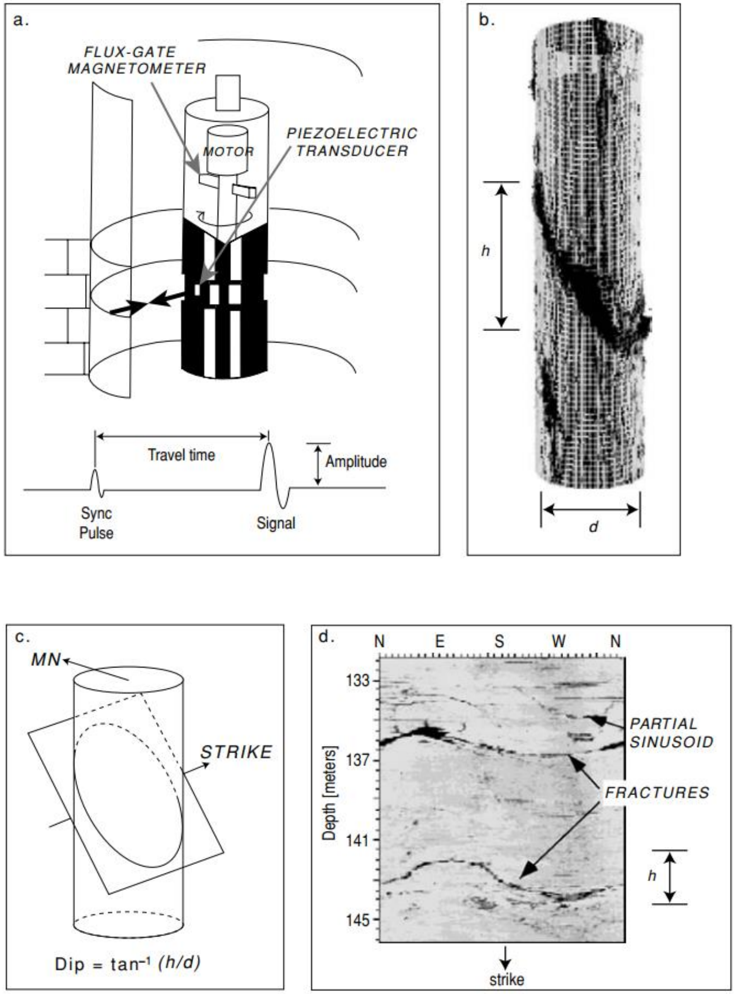

Zoback MD, 2007, Reservoir Geomechanics, Cambridge University Press

Wellbore Imaging
Ultrasonic borehole televiewer (BHTV)

- Ultrasonic borehole televiewer (BHTV) – Ultrasonic Borehole Imager (UBI)
  - Amplitude of the reflected pulse is diminished when the wellbore wall is rough (when there is a fracture)
    - Dip $\quad \text{Dip} = \tan^{-1}(h/d)$
    - Dip direction
  - Travel time increase when radius is increased
    - Used for borehole breakout analysis
  - (Apparent) aperture of fractures
    - What we see may not reflect what it is

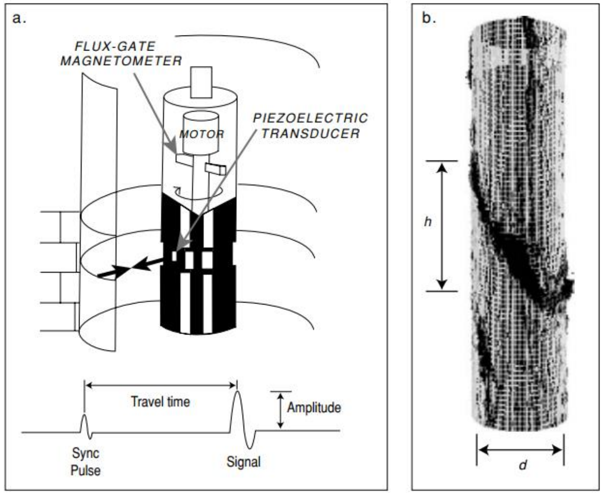

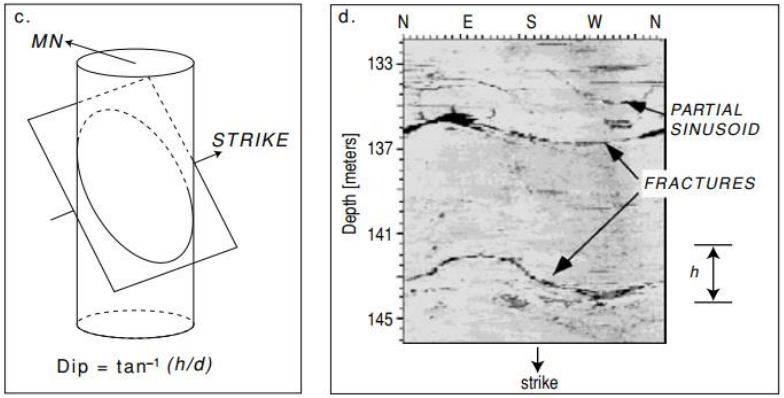

Dip direction?

Zoback MD, 2007, Reservoir Geomechanics, Cambridge University Press

Wellbore Imaging
Electrical Imaging device

- Electrical imaging device
  - Monitor the contact resistance (with four or six pad)
  - Fine-scale map of the wellbore wall with great precision
  - Less useful for size and shape

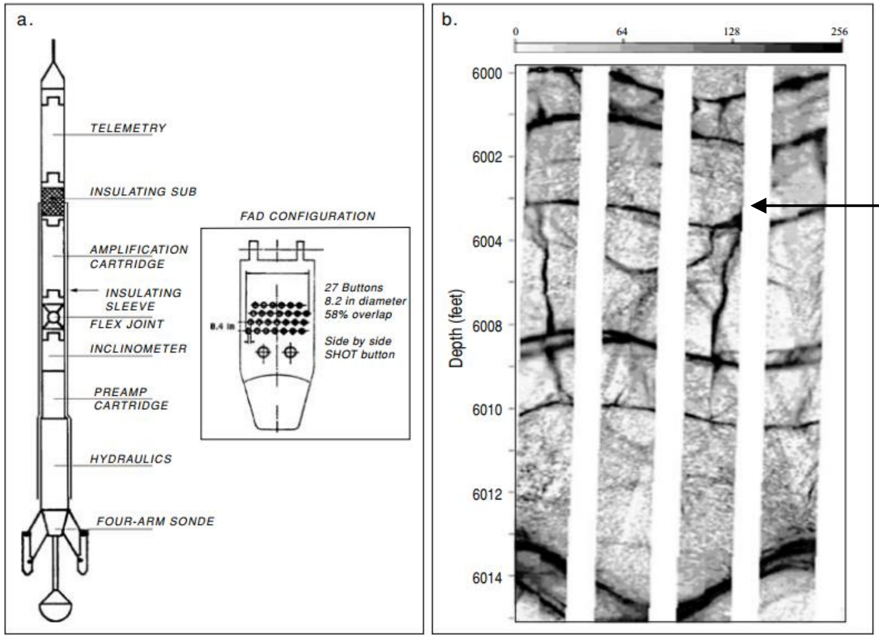

gap: no data at electrode node

Zoback MD, 2007, Reservoir Geomechanics, Cambridge University Press

Wellbore Imaging
Ultrasonic televiewer & electrical image

- Examples of borehole breakout
  - Ultrasonic vs electrical

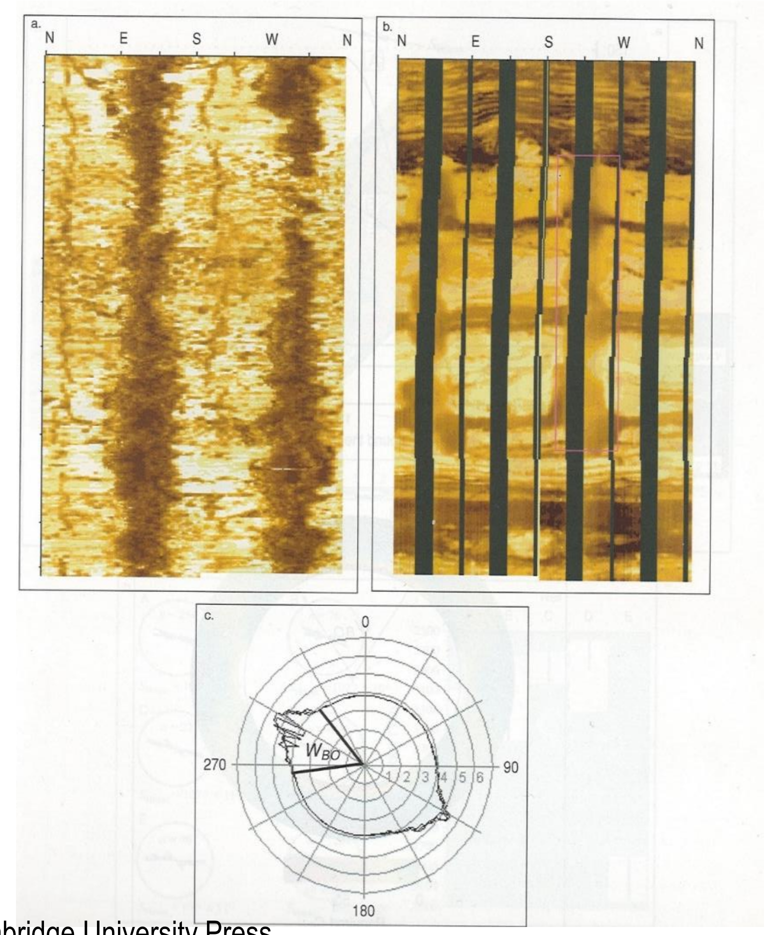

Zoback MD, 2007, Reservoir Geomechanics, Cambridge University Press

Wellbore Imaging
Characterizing Fractures

SEOUL NATIONAL UNIVERSITY

- Bias
  - Fracture characterization from vertical borehole
  - Imaging tool can underestimate the fracture whose planes are nearly parallel to borehole axis

fractures observed along a length of wellbore, $L = D/\cos\phi$, $N_{\mathrm{obs}}(\phi)$ must be corrected in order to obtain the true number of fractures that occur in the formation over a similar distance, $N_{\mathrm{true}}(\phi)$ via

$$N_{\mathrm{true}}(\phi) = (\cos\phi)^{-1} N_{\mathrm{obs}}(\phi) \tag{5.6}$$

Zoback MD, 2007, Reservoir Geomechanics, Cambridge University Press

3D Mohr diagrams

SEOUL NATIONAL UNIVERSITY

$$S^2 + \left(N - \frac{\sigma_2 + \sigma_3}{2}\right)^2 \geq \left(\frac{\sigma_2 - \sigma_3}{2}\right)^2$$

$$S^2 + \left(N - \frac{\sigma_1 + \sigma_3}{2}\right)^2 \leq \left(\frac{\sigma_3 - \sigma_1}{2}\right)^2$$

$$S^2 + \left(N - \frac{\sigma_1 + \sigma_2}{2}\right)^2 \geq \left(\frac{\sigma_1 - \sigma_2}{2}\right)^2$$

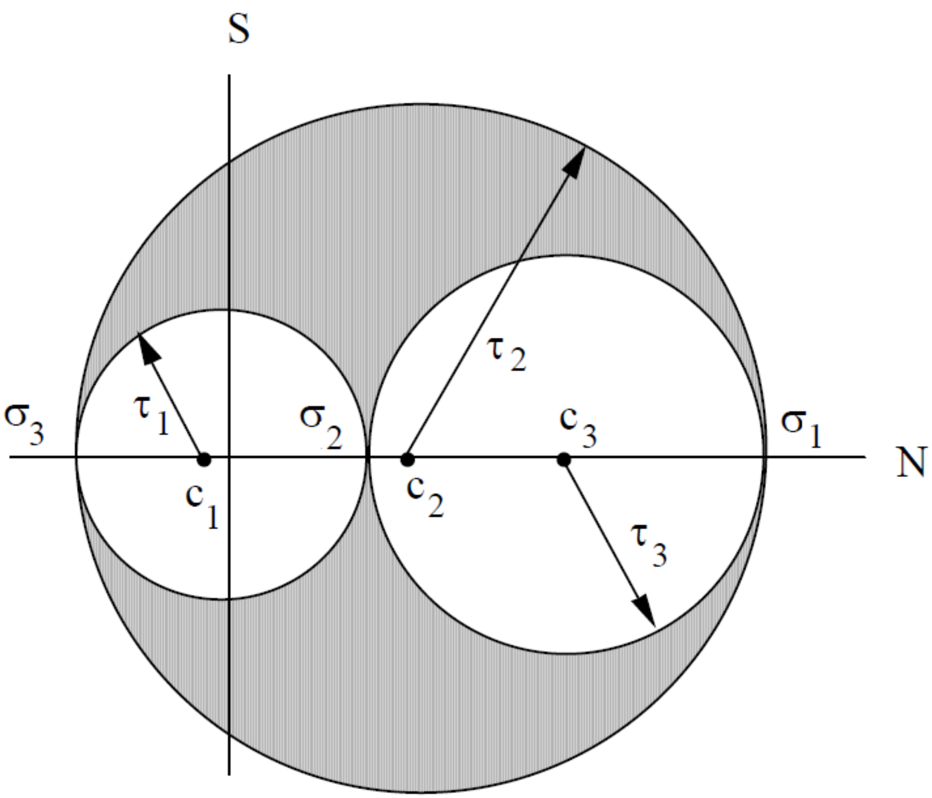

3D Mohr diagrams

SEOUL NATIONAL UNIVERSITY

- Graphical representation of 3D stress
  - Very useful for the evaluation of slip potential

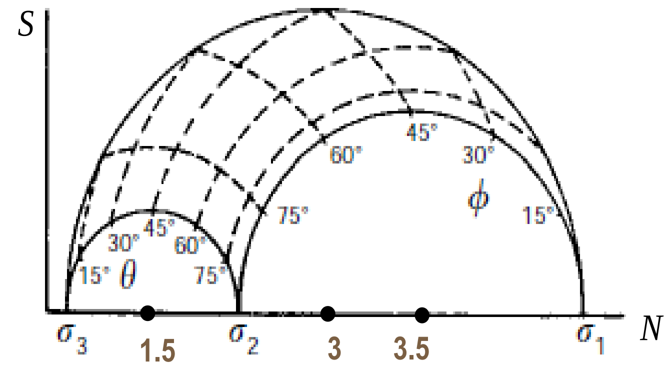

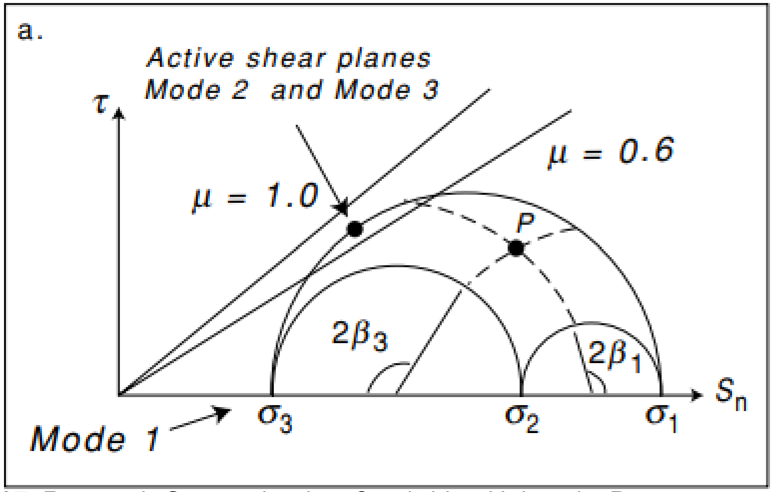

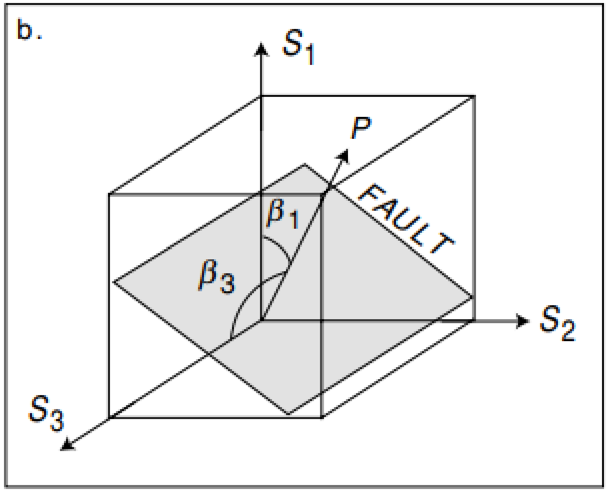

Zoback MD, 2007, Reservoir Geomechanics, Cambridge University Press

3D Mohr diagrams

- Stress Transformation (2D)

  - 전치행렬의 적용 예

    - Stress Transformation Equation

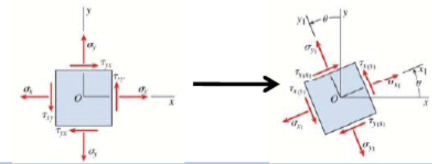

$$\sigma_{x_1} = \sigma_x \cos^2\theta + \sigma_y \sin^2\theta + 2\tau_{xy}\sin\theta\cos\theta \quad \textbf{or} \quad \sigma_{x_1} = \frac{\sigma_x+\sigma_y}{2} + \frac{\sigma_x-\sigma_y}{2}\cos 2\theta + \tau_{xy}\sin 2\theta$$

$$\tau_{x_1y_1} = -(\sigma_x-\sigma_y)\sin\theta\cos\theta + \tau_{xy}(\cos^2\theta-\sin^2\theta) \quad \textbf{or} \quad \tau_{x_1y_1} = -\frac{\sigma_x-\sigma_y}{2}\sin 2\theta + \tau_{xy}\cos 2\theta$$

    - Stress Transformation Equation using direction cosine (and its Transpose matrix)

$$\begin{pmatrix} \sigma_{x1} & \tau_{x1y1} \\ \tau_{x1y1} & \sigma_{y1} \end{pmatrix} = \begin{pmatrix} \cos\theta & \sin\theta \\ -\sin\theta & \cos\theta \end{pmatrix}\begin{pmatrix} \sigma_x & \tau_{xy} \\ \tau_{xy} & \sigma_y \end{pmatrix}\begin{pmatrix} \cos\theta & \sin\theta \\ -\sin\theta & \cos\theta \end{pmatrix}^T \qquad \boldsymbol{\tau}' = \mathbf{R}\boldsymbol{\tau}\mathbf{R}^{\mathrm{T}}$$

- Stress Transformation (3D)

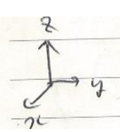

$$\underline{\underline{\tau}}' = \underline{\underline{R}}\,\underline{\underline{\tau}}\,\underline{\underline{R}}^T$$

$$\begin{pmatrix} \cos(x',x) & \cos(x',y) & \cos(x',z) \\ \cos(y',x) & \cos(y',y) & \cos(y',z) \\ \cos(z',x) & \cos(z',y) & \cos(z',z) \end{pmatrix} = \underline{\underline{R}}$$

3D Mohr diagrams
Useful for fracture slip potential

- Fault data from wellbore image analysis in highly fractured granite

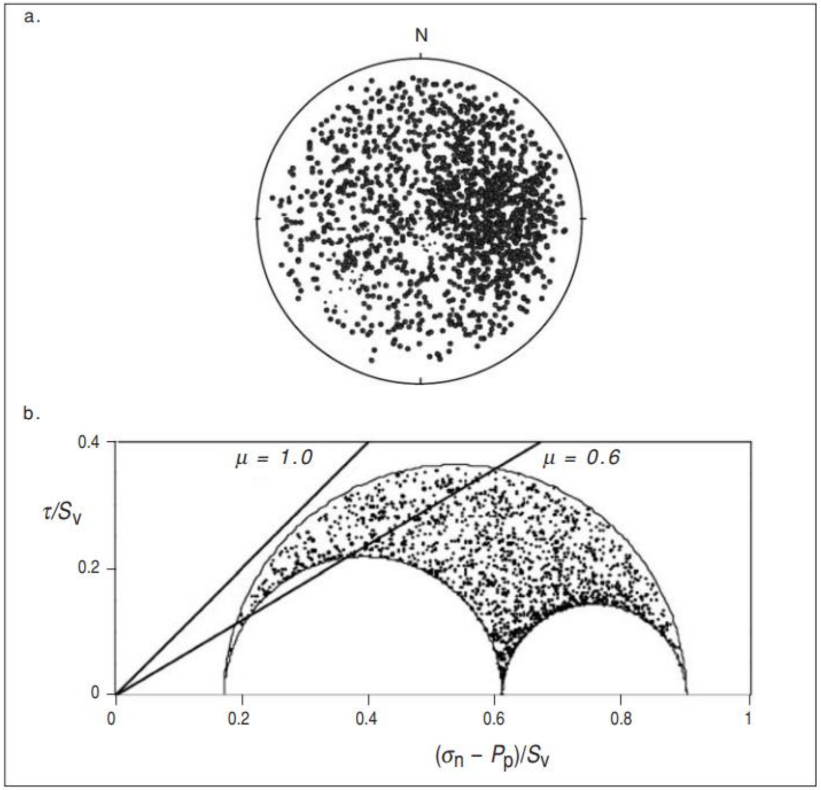

Figure 5.10. (a) Stereographic representation of fault data detected through wellbore image analysis in highly fractured granitic rock encountered in the Cajon Pass research well from 1750 to 3500 m depth (after Barton and Zoback 1992). (b) Representation of the same data utilizing a three-dimensional Mohr diagram normalized by the vertical stress. While many fractures appear to be critically stressed, most are not and thus reflect the rock's geologic history (after Barton, Zoback *et al.* 1995).

Zoback MD, 2007, Reservoir Geomechanics, Cambridge University Press

3D Mohr diagrams
Useful for fracture slip potential

- Critically stressed fractures tend to carry more fluid (hydrocarbon)

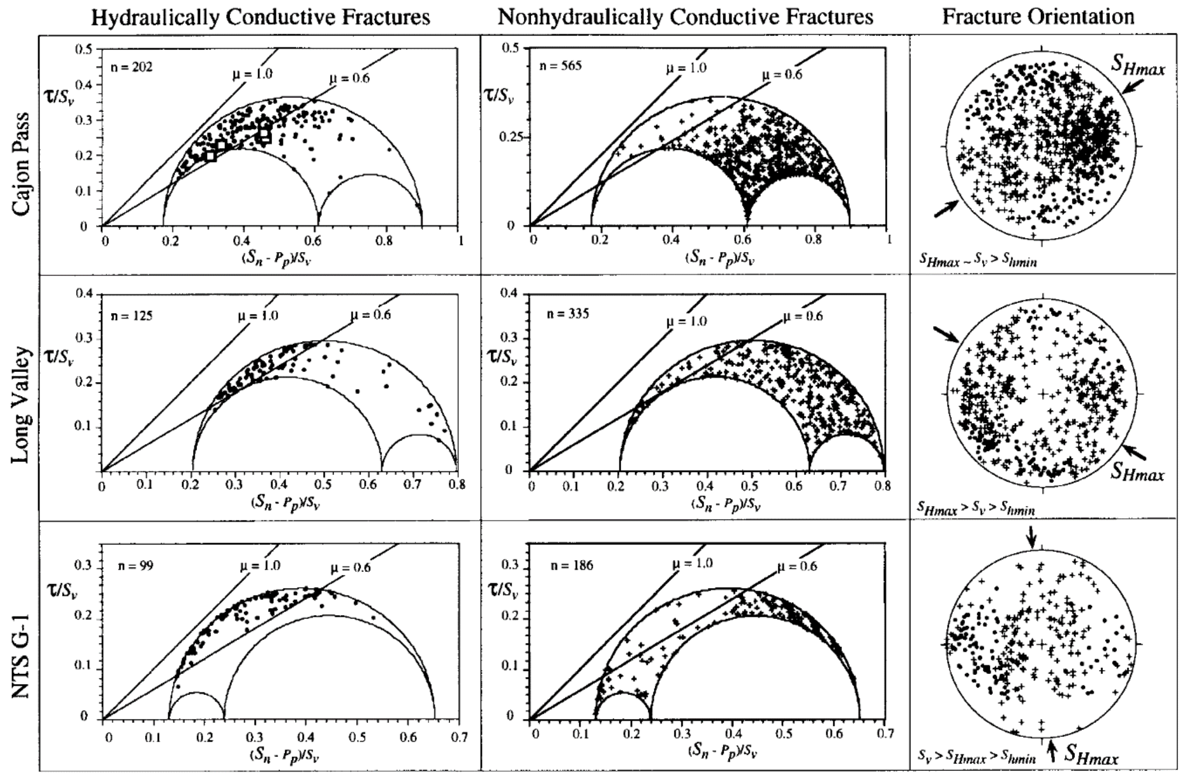

Figure 3. Normalized shear vs. effective normal stress for hydraulically conductive (left column) and nonhydraulically conductive (center column) fractures based on precision temperature logs (refer to Jaeger and Cook, 1979, p. 28, for details of construction of these diagrams). Open squares in upper left plot show stress state calculated for fractures in Cajon Pass borehole where flow was indicated by direct flow tests. Right column shows lower-hemisphere stereographic projections of poles to fracture planes for hydraulically conductive (solid circles) and nonhydraulically conductive (plus signs) planes.

Barton CA, Zoback MD, Moos D, 1995, Fluid flow along potentially active faults in crystalline rock. *Geology*;23(8):683-686.

Earthquake Focal Mechanisms

SEOUL NATIONAL UNIVERSITY

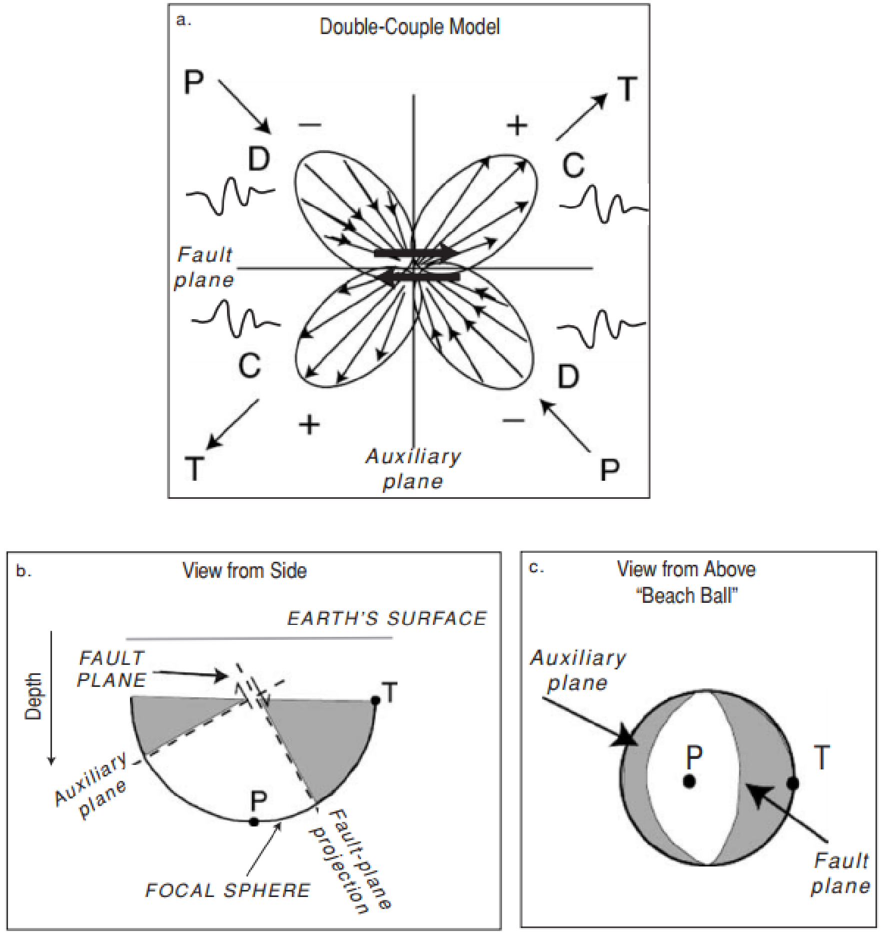

Figure 5.11. (a) Schematic illustration of the radiation pattern and force-couple associated with earthquakes as the basis earthquake focal plane mechanisms. An east–west striking, vertical right-lateral strike slip fault intersecting a half space is shown. The polarity of the P-waves defines the compressional and dilatational quadrants. (b) Cross-sectional view of the nodal planes, radiation pattern and *P*- and *T*-axes associated with an east-dipping normal fault. The radiation pattern does not uniquely distinguish the fault plane from the auxiliary plane. (c) Lower hemisphere stereonet representation of the normal faulting focal mechanism.

Zoback MD, 2007, Reservoir Geomechanics, Cambridge University Press

Earthquake Focal Mechanisms

SEOUL NATIONAL UNIVERSITY

- Focal mechanisms of earthquake
  - Provides the orientation of principal stresses using Coulomb failure criterion
  - Relative magnitude of the three principal stress
  - 77% of World Stress Map data
  - Based on the analysis of observed seismic waveform (first motion of P-wave). Upward: compression, downward: dilational

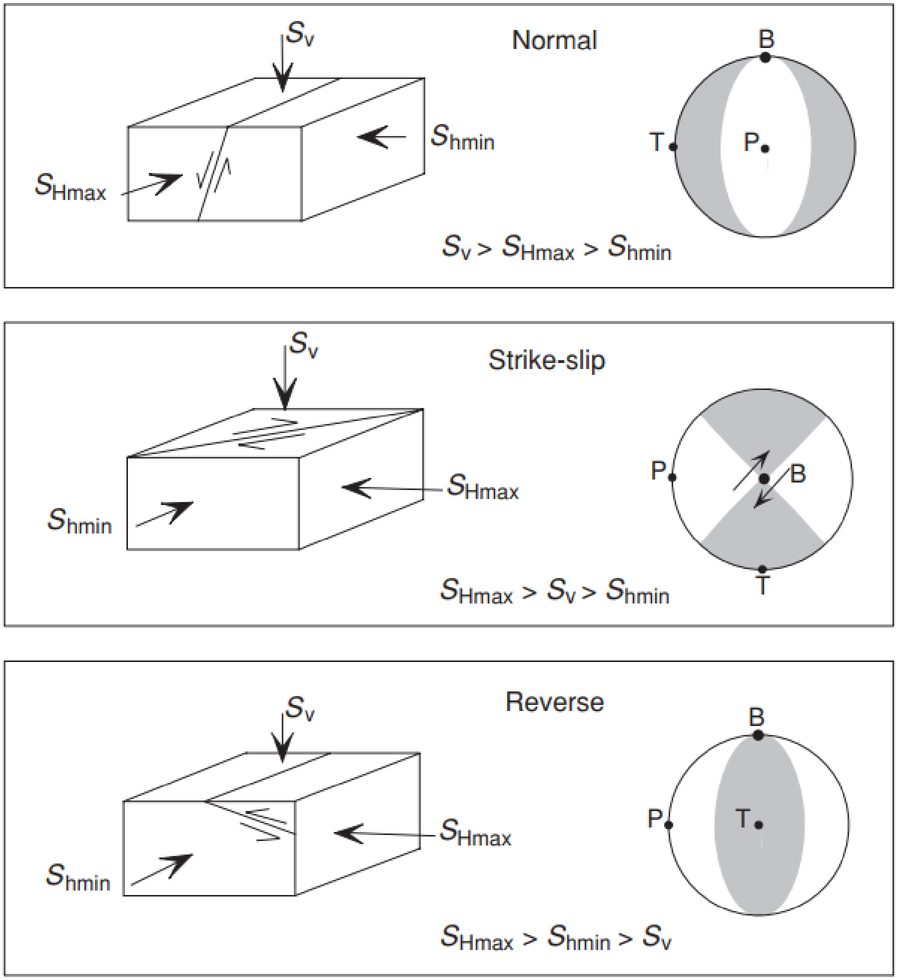

Figure 1.2. E. M. Anderson's classification scheme for relative stress magnitudes in normal, strike-slip and reverse faulting regions. Earthquake focal mechanisms, the *beach balls* on the right, are explained in Chapter 5.

Zang A, Stephansson O (2010) Stress field of the Earth's crust. Springer Science and Business Media BV, Dordrecht